Linear bioconvection in a suspension of randomly swimming, gyrotactic micro-organisms

M. A. Bees[a] and N. A. Hill
Department of Applied Mathematics, University of Leeds, Leeds LS2 9JT, United Kingdom

(Received 29 January 1998; accepted 30 April 1998)

We have analyzed the initiation of pattern formation in a layer of finite depth for Pedley and Kessler's new model [J. Fluid Mech. **212**, 155 (1990)] of bioconvection. This is the first analysis of bioconvection in a realistic geometry using a model that deals with random swimming in a rational manner. We have considered the effects of a distribution of swimming speeds, which has not previously received attention in theoretical papers and find that it is important in calculating the diffusivity. Our predictions of initial pattern wavelengths are reasonably close to the observed ones but better experimental measurements of key parameters are needed for a proper comparison. © *1998 American Institute of Physics.* [S1070-6631(98)02808-6]

I. INTRODUCTION

Far from being a recently discovered phenomenon, patterns in suspensions of swimming cells have been observed for some time. Ever since common algae, such as *Chlamydomonas nivalis*, *Euglena viridis*, *Crypthecodinium cohnii* and the ciliated protozoan *Tetrahymena pyriformis* were isolated, plumes of aggregating cells have been noticed in the culturing flasks. Platt[1] coined the term ''bioconvection'' to describe the phenomenon of pattern formation in shallow suspensions of motile micro-organisms at constant temperature, on a par with those found in convection experiments. However, this is by no means the first documented observation, which goes back to at least 1848 (e.g., Wager[2]). Other experimental investigators have included Loeffer and Mefferd,[3] Nultsch and Hoff,[4] Plesset and Winet[5] and, more recently, Kessler,[6,7] Bees[8] and Bees and Hill.[9] Bioconvection is generally due to an overturning instability caused by micro-organisms swimming to the upper surface of a fluid which has a lower density than the micro-organisms.

The first models of bioconvection were developed by Plesset and Winet.[5] They considered a Rayleigh-Taylor instability in a continuously stratified, two-layer model and were able to investigate the preferred pattern wavelength as a function of the upper layer depth and the cell concentration. Levandowsky *et al.*[10] investigated bioconvection patterns and proposed a more realistic model (Childress *et al.*[11]) in which the micro-organisms could swim but were constrained to swim upwards only, due to their asymmetric density distribution. As density fluctuations in the suspension are generally small, they assumed that variations in viscosity due to the concentration of cells and the possible effects on the stress tensor due to the swimming motion of the micro-organisms are both negligible. Their application of the Boussinesq approximation implies that the only way in which the cell concentration can affect the fluid flow is through vertical variations in the fluid density. In experiments with *C. nivalis* (a biflagellate alga), Kessler[6,7,12] first realized the importance of hydrodynamic focusing within flows. Kessler termed the biological component of this process gyrotaxis, which occurs as a result of the balance between viscous and gravitational torques exerted on the cell. Its effect is to tip a swimming cell away from the vertical so that its preferred swimming direction is towards regions of down-welling fluid and away from regions of up-welling fluid. A deterministic approach was used in the models of Pedley *et al.*,[13] for a suspension of infinite depth, and Hill *et al.*,[14] for a suspension of finite depth. However, Pedley and Kessler[15] later reasoned that by considering the cell diffusion tensor, **D**, as isotropic and, hence, ''strongly random'' and independent of the mechanisms involved in gyrotaxis, Pedley *et al.*[13] were being inconsistent in that they were considering the determination of the swimming velocity, $\mathbf{V}_s$, as ''weakly random.'' That is to say that calculating the cell swimming direction, in a deterministic manner, for all of the cells, and then assuming that there was no bias in the direction of diffusion of these cells was inconsistent. Therefore, instead of assuming a constant orthotropic diffusion tensor (as in Childress *et al.*[11]) they modeled the cell swimming direction in a probabilistic fashion. A model analogous to that of suspensions of colloidal particles subject to rotary Brownian motion (Brenner and Weissmann and Brenner;[16–18] Hinch and Leal and Leal and Hinch[19–22]) was applied. From this, they calculated the average swimming direction and the cell diffusion tensor. We shall adopt the approach of Pedley and Kessler[15] and use an analysis similar to that of Hill *et al.*[14] to investigate bioconvection in a suspension of finite depth.

Our aim in this paper is to predict a particular most unstable mode (i.e., one that grows most rapidly) from an initial equilibrium solution (in the spirit of Chandrasekar[23]). This can be compared, in principle, with the experiments of Bees and Hill[9] and with the deterministic theoretical predictions of Hill *et al.*[14] In experiments, however, it is sometimes

[a]Present address: Center for Chaos and Turbulence Studies, Physics Institute, Denmark's Technical University, Bygning 309, DK-2800 Lyngby, Copenhagen, Denmark; Electronic mail: Martin.A.Bees@fysik.dtu.dk

difficult to realize the very first unstable linear mode before nonlinear effects become significant (Bees and Hill[9]).

An equilibrium solution, of the full equations for finite depth and zero flow, is found and is then perturbed, allowing weak ambient flow. Brenner and Weissmann[16] describe the use of asymptotic expansions in their analysis of a Fokker-Planck equation to describe dipolar spheres subject to external couples and rotational Brownian motion which was extended by Pedley and Kessler[15] for their infinite-depth model. For a suspension of infinite depth, the first order correction to the diffusion tensor did not appear in the full linear equations. However, in the finite depth case, the first order diffusion tensor is of paramount importance and can control the range of unstable wavenumbers.

The full linear equations are solved using asymptotic and numerical techniques for a finite depth, in a similar manner to Hill *et al.*,[14] with the added complications of the nonconstant diffusion and mean cell swimming velocity which are modeled using the Fokker-Planck equation. Hillesdon *et al.*[24] and Hillesdon[25] investigate patterns formed by chemotactic (or more specifically aerotactic) bacteria and some of their analytic and numerical techniques stem from the same sources as those contained in this paper. In their model the analysis is further complicated by discontinuities in the bacterial concentration gradient and ideas from the theory of penetrative convection (Veronis[26]) had to be employed to understand the nonlinear behavior of the system. However, their model does not include coupling of fluid flow and cell orientation in a Fokker-Planck equation. Vincent and Hill[27] study an additional instability due to a typical phototactic response, for which they predict a range of steady and oscillatory behavior in a suspension of swimming microorganisms.

Finally, we investigate the effect of modeling the swimming speed as a random variable and compare our predictions with the experiments of Bees and Hill.[9]

II. MODEL FORMULATION

Following the continuum model of Pedley and Kessler,[15] for a dilute suspension of swimming cells, the suspension is incompressible so that

$$\nabla \cdot \mathbf{u} = 0, \tag{1}$$

where $\mathbf{u}(\mathbf{x})$ is the velocity of the suspension, and using the Boussinesq approximation the momentum equation is

$$\rho \frac{D\mathbf{u}}{Dt} = -\nabla p_e + nv\Delta\rho\mathbf{g} + \mu\nabla^2\mathbf{u}. \tag{2}$$

Here $n(\mathbf{x})$ is the local cell concentration, μ is the fluid viscosity, $p_e(\mathbf{x})$ is the excess pressure, v is the mean volume of a cell, and $\Delta\rho$ is the difference between the cell and fluid density, ρ. The total number of cells is conserved so that

$$\frac{\partial n}{\partial t} = -\nabla \cdot [n(\mathbf{u} + V_s\langle \mathbf{p} \rangle) - \mathbf{D} \cdot \nabla n], \tag{3}$$

where $\langle \mathbf{p}(\mathbf{x}) \rangle$ is the mean cell direction, V_s is the mean cell swimming speed and $\mathbf{D}(\mathbf{x})$ is the cell diffusion tensor. The boundary conditions for a suspension trapped between two rigid horizontal boundaries are that of no-slip,

$$\mathbf{u} = \mathbf{0}, \quad \text{at } z = 0, -H, \tag{4}$$

and that of zero cell flux perpendicular to the boundaries

$$\mathbf{k} \cdot [n(\mathbf{u} + V_s\langle \mathbf{p} \rangle) - \mathbf{D} \cdot \nabla n] = 0, \quad \text{at } z = 0, -H. \tag{5}$$

Here $\mathbf{k}$ is a unit vector directed vertically upwards. An equilibrium solution to the above equations is

$$\mathbf{u} = \mathbf{0}, \quad n = Ne^{\kappa z}, \quad \langle \mathbf{p} \rangle = \langle \mathbf{p} \rangle^0 \text{ and } \mathbf{D} = \mathbf{D}^0, \tag{6}$$

where

$$\kappa = \frac{V_s \langle \mathbf{p} \rangle_3^0}{D_{33}^0}, \tag{7}$$

the subscript 3 indicating components in the vertical direction. κ^{-1} represents a local scale height. From the normalization condition,

$$\int_{-H}^{0} n\,dz = H\overline{n}, \tag{8}$$

where $\overline{n}$ is the mean cell concentration and $n = Ne^{\kappa z}$, it follows that

$$N = \frac{H\overline{n}\kappa}{1 - e^{-\kappa H}}. \tag{9}$$

The cell swimming direction probability density function (p.d.f.) defined on the unit sphere is $f(\mathbf{p})$, where

$$\mathbf{p} = (\sin\theta\cos\phi, \sin\theta\sin\phi, \cos\theta)^T, \tag{10}$$

and θ and ϕ are spherical polar angles. θ is the colatitude measured relative to $\mathbf{k}$. The mean cell swimming direction, $\langle \mathbf{p} \rangle$, is defined by

$$\langle \mathbf{p} \rangle = \int_S \mathbf{p} f(\mathbf{p})\,dS, \tag{11}$$

where S is the surface of the unit sphere and

$$\mathbf{D}(t) = \int_0^\infty \langle \mathbf{V}_r(t)\mathbf{V}_r(t - t') \rangle dt'. \tag{12}$$

Here $\mathbf{V}_r$ is the velocity of a cell relative to its mean value. (See Shu *et al.*[28] for a further discussion of this formula.) The expression for $\mathbf{D}$ is, of course, hard to calculate as it requires a knowledge of all previous cell velocities and, hence, we are forced to make an approximation for the sake of simplicity. If the cell swimming speed, V_s, is a constant as assumed by Pedley and Kessler[15] (the effects of a nonconstant V_s on the linear analysis will be considered in Sec. VI) and if it is assumed that there exists a direction correlation time-scale, τ, such that the cell's direction changes by less than a specified angle, then we may write

$$\mathbf{D} \approx V_s^2 \tau \langle (\mathbf{p} - \langle \mathbf{p} \rangle)(\mathbf{p} - \langle \mathbf{p} \rangle) \rangle. \tag{13}$$

Essentially, τ can be determined from experiments (Pedley and Kessler;[15] Hill and Häder[29]) to be approximately equal to 1.3 s. Shu *et al.*[28] discuss this approximation in greater detail. Equation (13) has been successfully employed before by Pedley and Kessler,[15] Bees[8] and Bees and Hill.[30] The p.d.f., $f(\theta, \phi)$, satisfies the Fokker-Planck conservation equation,

$$\frac{\partial f}{\partial t}+\boldsymbol{\nabla}\cdot(\dot{\mathbf{p}}f)=D_r\nabla^2 f, \tag{14}$$

where D_r is a constant rotational diffusivity that incorporates rotational Brownian effects and the intrinsically imperfect locomotion of the cells (see Pedley and Kessler;[15] Risken;[31] Schienbein and Gruler[32]). D_r is an unknown constant. It can be estimated from the data of Hill and Häder[29] to be 0.065 s^{-1} (see Pedley and Kessler;[33] Bees[8]).

From the dimensional torque balance equation for gyrotactic cells (Pedley and Kessler[15]),

$$\dot{\mathbf{p}}=\frac{1}{2B}[\mathbf{k}-(\mathbf{k}\cdot\mathbf{p})\mathbf{p}]+\frac{1}{2}\boldsymbol{\Omega}\wedge\mathbf{p}+\alpha_0\mathbf{p}\cdot\mathbf{E}\cdot(\mathbf{I}-\mathbf{pp}), \tag{15}$$

where B is the gyrotactic reorientation time-scale of a cell affected by external (gravitational) torques subject to resisting viscous torques, given by

$$B=\frac{\mu\alpha_\perp}{2h\rho g}, \tag{16}$$

where h is the center-of-mass offset relative to the geometrical center of the cell and $\alpha_\perp$ is the dimensionless resistance coefficient for rotation about an axis perpendicular to $\mathbf{p}$ (Table II; Pedley and Kessler,[15] Appendix A). $\boldsymbol{\Omega}$ and $\mathbf{E}$ are the local vorticity vector and rate-of-strain tensor, respectively.

Nondimensionalizing such that

$$\boldsymbol{\Omega}=\frac{V_s^2\tau}{H^2}\boldsymbol{\omega}\ \text{ and }\ \mathbf{E}=\frac{V_s^2\tau}{H^2}\mathbf{e}, \tag{17}$$

and substituting into the steady form of the Fokker-Planck equation (14) gives (see Bees[8] for details)

$$\mathbf{k}\cdot\boldsymbol{\nabla}f-2(\mathbf{k}\cdot\mathbf{p})f+\eta\boldsymbol{\omega}\cdot(\mathbf{p}\wedge\boldsymbol{\nabla}f)+2\eta\alpha_0[\mathbf{p}\cdot\mathbf{e}\cdot\boldsymbol{\nabla}f-3\mathbf{p}\cdot\mathbf{e}\cdot\mathbf{p}f\ ]=\lambda^{-1}\nabla^2 f, \tag{18}$$

where

$$\lambda=\frac{1}{2D_rB} \tag{19}$$

and

$$\eta=\frac{BV_s^2\tau}{H^2}. \tag{20}$$

(Note: λ differs by a factor of $\frac{1}{2}$ omitted in error in Pedley and Kessler[15] but corrected in the Pedley and Kessler review.[33]) Here, η is called the dimensionless gyrotaxis parameter and α_0 is the cell eccentricity given by

$$\alpha_0=\frac{a^2-b^2}{a^2+b^2}, \tag{21}$$

where a and b are the major and minor dimensions of a cell respectively.

Using our best estimates (see Table II later) $\lambda=2.2$ and $\eta=1.8\times10^{-4}\times H^{-2}$ where H is the depth of the layer in cm (or $\eta=33d^{-2}$; see later).

Lengths are scaled on H, the depth of the suspension, cell concentration on N and diffusivity on $V_s^2\tau$, where V_s is the cell swimming speed and τ is the direction correlation time, and the time-scale for the flow is $H^2/V_s\tau$ so that the nondimensionalized governing equations become

$$\boldsymbol{\nabla}\cdot\mathbf{u}=0, \tag{22}$$

$$S_c^{-1}\frac{D\mathbf{u}}{Dt}=-\boldsymbol{\nabla}p_e-\gamma n\mathbf{k}+\nabla^2\mathbf{u} \tag{23}$$

and

$$\frac{\partial n}{\partial t}=-\boldsymbol{\nabla}\cdot\left[n\mathbf{u}+d\frac{K_2}{K_1}n\langle\mathbf{p}\rangle-\mathbf{D}\cdot\boldsymbol{\nabla}n\right], \tag{24}$$

where

$$d=H\kappa=\frac{K_1H}{K_2V_s\tau} \tag{25}$$

is the ratio of layer depth, H, to sublayer depth, κ^{-1}. K_1 and K_2 are functions of λ and are given in the appendix. For $d\gg1$ we have a ''deep suspension,'' and for $d\ll1$ we have a ''shallow suspension.'' The Schmidt and Rayleigh numbers are defined as

$$S_c=\frac{\nu}{V_s^2\tau} \tag{26}$$

and

$$R=\gamma d=\frac{Nvg\Delta\rho H^4K_1}{\nu\rho V_s^3\tau^2K_2}. \tag{27}$$

R is based on the total depth of the layer. The equilibrium state, the stability of which we shall investigate, is $\mathbf{u}=\mathbf{0}$, $\langle\mathbf{p}\rangle=\langle\mathbf{p}\rangle^0$, $n=e^{dz}$ and $\mathbf{D}=\mathbf{D}^0$ in nondimensional variables.

III. LINEAR ANALYSIS

The solution of the Fokker-Planck equation for weak flow is given in Pedley and Kessler[15] in terms of associated Legendre polynomials (see also Bees *et al.*[30] for more general solutions). We will employ this solution for the linear analysis in a suspension of finite depth later in this section and, hence, we summarize the results here and define the constants in Appendix A. In particular, we correct an error in the calculation of K_4 which appeared in Pedley and Kessler (Appendix B).[15]

Consider a perturbation from the equilibrium solution for a suspension of finite depth by setting

$$\mathbf{u}=\epsilon\mathbf{u}^1,\quad \langle\mathbf{p}\rangle=\langle\mathbf{p}\rangle^0+\epsilon\langle\mathbf{p}\rangle^1,\quad n=e^{dz}+\epsilon n^1,\quad p_e=p_e^0+\epsilon p_e^1,\quad \mathbf{D}=\mathbf{D}^0+\epsilon\mathbf{D}^1, \tag{28}$$

where $\epsilon\ll1$. The mean cell swimming direction is given by

$$\langle\mathbf{p}\rangle=(0,\ 0,\ K_1)^T+\epsilon\left[\eta J_1(\omega_2^1,\ -\omega_1^1,\ 0)^T-2\alpha_0\eta\left(e_{13}^1J_4,\ e_{23}^1J_4,\ \frac{3}{2}e_{33}^1K_4\right)^T\right]+O(\epsilon^2), \tag{29}$$

where $\boldsymbol{\omega}=\epsilon\boldsymbol{\omega}^1$ and $\mathbf{e}=\epsilon\mathbf{e}^1$, and the diffusion tensor is calculated from Eq. (13) to be

$$\frac{1}{V_s^2\tau}\mathbf{D}=\begin{pmatrix}\frac{K_1}{\lambda} & 0 & 0\\ 0 & \frac{K_1}{\lambda} & 0\\ 0 & 0 & K_2\end{pmatrix}+\epsilon\left[\eta(J_2-J_1K_1)\begin{pmatrix}0 & 0 & \omega_2^1\\ 0 & 0 & -\omega_1^1\\ \omega_2^1 & -\omega_1^1 & 0\end{pmatrix}\right.$$

$$\left.-2\alpha_0\eta\begin{pmatrix}-\frac{3}{4}e_{33}^1K_5+\frac{1}{4}(e_{11}^1-e_{22}^1)J_6 & \frac{1}{2}e_{12}^1\ J_6 & e_{13}^1(J_5-K_1J_4)\\ \frac{1}{2}e_{12}^1\ J_6 & -\frac{3}{4}e_{33}^1K_5-\frac{1}{4}(e_{11}^1-e_{22}^1)J_6 & e_{23}^1(J_5-K_1J_4)\\ e_{13}^1(J_5-K_1J_4) & e_{23}^1(J_5-K_1J_4) & \frac{3}{2}e_{33}^1(K_5-2K_1K_4)\end{pmatrix}\right]+O(\epsilon^2). \tag{30}$$

The constants K_1 to K_5 and J_1 to J_5 are defined in Appendix A.

The governing system of equations is then reduced to the two equations (as described in Appendix A),

$$S_c^{-1}\frac{\partial}{\partial t}(\nabla^2u_3^1)=\nabla^4u_3^1-\gamma\nabla^2n^1+\gamma\partial_3^2n^1 \tag{31}$$

and

$$\frac{\partial n^1}{\partial t}=de^{dz}\{-1+\eta P_7\nabla^2+\eta[P_5-P_7]\partial_3^2+\eta dP_6\partial_3\}u_3^1$$
$$+\{P_H\nabla^2+(P_V-P_H)\partial_3^2-dP_v\partial_3\}n^1, \tag{32}$$

in terms of the independent variables n^1 and u_3^1 only, where

$$P_V=K_2,\quad P_H=\frac{K_1}{\lambda}, \tag{33}$$

$$P_5=J_1\left(K_1+\frac{K_2}{K_1}\right)-J_2-\left[J_4\left(K_1+\frac{K_2}{K_1}\right)-J_5\right]\alpha_0$$
$$+3\left[K_4\left(2K_1+\frac{K_2}{K_1}\right)-K_5\right]\alpha_0,$$

$$P_6=3\left[K_4\left(2K_1+\frac{K_2}{K_1}\right)-K_5\right]\alpha_0$$

and

$$P_7=J_1\left(K_1+\frac{K_2}{K_1}\right)-J_2+\left[J_4\left(K_1+\frac{K_2}{K_1}\right)-J_5\right]\alpha_0. \tag{34}$$

We consider normal mode solutions of the form

$$u_3^1=W(z)e^{i(lx+my)+\sigma t}\ \text{ and }\ n^1=\Phi(z)e^{i(lx+my)+\sigma t}. \tag{35}$$

On substitution into (31) and (32), we get

$$\left(\frac{\sigma}{S_c}+k^2-\frac{d^2}{dz^2}\right)\left(k^2-\frac{d^2}{dz^2}\right)W=-Rd^{-1}k^2\Phi \tag{36}$$

and

$$\left(P_V\frac{d^2}{dz^2}-P_Vd\frac{d}{dz}-P_Hk^2-\sigma\right)\Phi$$
$$=de^{dz}\left[1-\eta P_5\frac{d^2}{dz^2}-\eta P_6d\frac{d}{dz}+\eta P_7k^2\right]W, \tag{37}$$

where $k=\sqrt{l^2+m^2}$ and the P_i are functions of the parameter $\lambda=(2D_r\ B)^{-1}$ and linear functions of the shape parameter α_0 as defined in (34). See the Appendix for more details.

The boundary conditions (4) and (5) become

$$W=0,\quad \frac{dW}{dz}=0,\ \text{and}\ \ \Phi d-\frac{d\Phi}{dz}=0,\ \text{on}\ \ z=0,-1. \tag{38}$$

The exponential appearing in Eq. (37) prevents an explicit solution from being found and we must resort to finding asymptotic or numerical solutions.

IV. ASYMPTOTIC ANALYSIS

The work in this section uses similar techniques to those in Hill *et al.*[14] for the earlier continuum model. If we assume, for example, that *C. nivalis* is a self-propelled spheroid and correspondingly $\lambda=2.2$ and $\alpha_0=0.31$ then

$$P_V\approx0.16,\quad P_H\approx0.26, \tag{39}$$

$$P_5\approx0.21,\quad P_6\approx-0.035\ \text{ and }\ P_7\approx0.19. \tag{40}$$

P_6 appears to be too small to be classed as $O(1)$ but by noting that P_5, P_6 and P_7 always appear in Eq. (37) multiplied by η (and $\eta\approx33d^{-2}$; see below) then it simplifies matters to consider $P_i=O(1)$ and $\eta=O(d^n)$ for some n and $i=5,6,7$. This assumption is justified asymptotically provided we either assume that d is much smaller than P_i for all i for shallow layers or much larger for deep layers. Using the definition of d and Eq. (20) we can write

$$\eta=\frac{BK_1^2}{\tau K_2^2}d^{-2}\approx33d^{-2}, \tag{41}$$

where we have used $B=3.4$ and $\tau=1.3$.

There are two natural asymptotic expansions which could be considered here: one for small d and one for large values. Note that since Eq. (25) implies

TABLE I. Values of the K and J constants, for varying values of λ, from Pedley and Kessler (Ref. 15) with corrections for K_4.

λ	K_1	K_2	K_3	K_4	K_5
0.3	0.099	0.0059	0.33	−0.0039	−0.013
1.0	0.31	0.061	0.28	−0.037	−0.048
2.2	0.57	0.22	0.16	−0.10	−0.11
3.0	0.67	0.33	0.10	−0.12	−0.14
λ	J_1	J_2	J_4	J_5	J_6
0.3	0.015	7.4×10^{-4}	-4.6×10^{-3}	−0.02	−0.040
1.0	0.14	0.024	−0.064	−0.064	−0.12
2.2	0.45	0.16	−0.26	−0.13	−0.20
3.0	0.60	0.27	−0.41	−0.18	−0.22

TABLE III. The values of the constants P for typical values of λ and α_0.

α_0	λ	P_5	P_6	P_7	P_H	P_V
0.0	2.2	0.22	0.0	0.22	0.26	0.16
0.2	0.3	0.050	−0.00017	0.050	0.33	0.33
0.2	1.0	0.14	−0.0050	0.14	0.31	0.28
0.2	2.2	0.22	−0.022	0.20	0.26	0.16
0.2	3.0	0.23	−0.028	0.19	0.22	0.10
0.31	2.2	0.21	−0.035	0.19	0.26	0.16
0.40	2.2	0.21	−0.044	0.18	0.26	0.16
1.00	2.2	0.20	−0.11	0.13	0.26	0.16

$$H=\frac{K_2 V_s \tau d}{K_1}, \tag{42}$$

then, from Tables I and II, $H=23d$ μm and so, if $d=0.1$, then the depth of the fluid is equal to 2.3 μm, which is very small for a fluid layer. A typical experimental depth of 5 mm gives $d=220$ (2 s.f.), for which the large d expansion should be valid. The small d expansion, however, is used to validate the numerical solutions in the next section. We compute other values of the P_i's in Table III for a range of λ and α_0.

A. Shallow layer analysis ($0<d\ll1$)

This case is similar to the shallow layer analysis of Hill *et al.*[14] and, therefore, we quote the results in Appendix B and merely give a brief description below (see Bees[8] for the details).

Suppose that the pattern wavelength is comparable with the sublayer depth and set $\tilde{k}=k/d$ where $\tilde{k}\sim1$. There are six boundary conditions which imply that we need to keep the highest order derivatives. The leading order balance in Eq. (36) must be

TABLE II. Parameter estimates and measurements (Refs. 14,15,29,34).

Name	Description	Typical value	Units
Length scale	Average cell diameter	10	μm
Length scale	Cell spacing	100	μm
Length scale	Convection patterns	0.2–2.0	cm
D	Diffusivity	5×10^{-5}–5×10^{-4}	cm^2/s
ρ	Fluid density	1	gm/cm^3
$\rho+\Delta\rho$	Cell density	1.05	gm/cm^3
v	Cell volume	5×10^{-10}	cm^3
h	Center of gravity offset	0–0.5	μm
α_0	Cell eccentricity	0.20–0.31	
α_0	Including flagella	0.40	
$\alpha_\perp$	Viscous torque parameter	6.8	
V_s	Cell swimming speed	63	μm/s
μ	Dynamic viscosity	10^{-2}	gm/cm s
g	Acceleration due to gravity	10^3	cm/s^2
λ	Small ⇒ random behavior Large ⇒ deterministic	2.2	
τ	Direction correlation time	1.3	s
B	Gyrotaxis parameter	3.4	s
B	Including flagella	6.3	s
D_r	Cells' rotational diffusivity	0.067	s^{-1}
S_c	Schmidt number	19	

$$\left(D^2-\frac{\sigma}{S_c}\right)D^2W=-d\tilde{k}^2R\Phi. \tag{43}$$

Otherwise we obtain the trivial solution. Here and henceforth $D\equiv d/dz$. Without loss of generality, we shall always assume $\Phi\sim1$ and hence $W\sim dR$. Close to neutrally stable solutions we can neglect σ and there are then four nontrivial leading order balances of Eq. (37) to be considered.

• **CASE I**

$$D^2\Phi=0, \tag{44}$$

which implies $R\ll O(d^{-2})$ and $\eta R\ll O(d^{-2})$.

• **CASE II**

$$P_V D^2\Phi=dW, \tag{45}$$

which implies $R\sim d^{-2}$ and $\eta R\ll O(d^{-2})$.

• **CASE III**

$$P_V D^2\Phi=d[W-\eta P_5 D^2W], \tag{46}$$

which implies $R\sim d^{-2}$ and $\eta R\sim d^{-2}$.

• **CASE IV**

$$P_V D^2\Phi=-d\eta P_5 D^2W, \tag{47}$$

which implies $R\ll O(d^{-2})$ and $\eta R\sim d^{-2}$.

This is summarized in Fig. 1. Case III leads to numerical analysis with a measure of complexity similar to that of the full problem and so this case has not been considered here.

B. Deep layer analysis ($d\gg1$)

Consider the case where $\sigma=0$ and $k\sim1$ where d^{-1} is small; then

$$(D^2-k^2)^2W=-k^2d^{-1}R\Phi \tag{48}$$

and

$$(P_V D^2-P_V dD-P_H k^2)\Phi = de^{dz}[1-\eta P_5 D^2-\eta d P_6 D+\eta P_7 k^2]W. \tag{49}$$

These equations are singular for large values of d and therefore we require a solution within the boundary layer at the top which can be matched to a solution for the outer region. For the outer solution the cell concentration is exponentially small, so that

$$(P_V D^2-P_V dD-P_H k^2)\Phi=0, \tag{50}$$

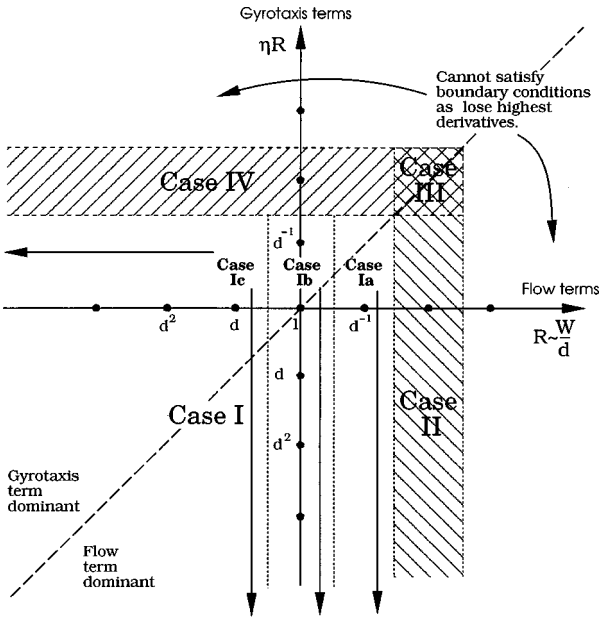

FIG. 1. Regions of the parameter space covered by the leading order balances of the linear equations for bioconvection in a shallow layer ($d \ll 1$). There are four major balances.

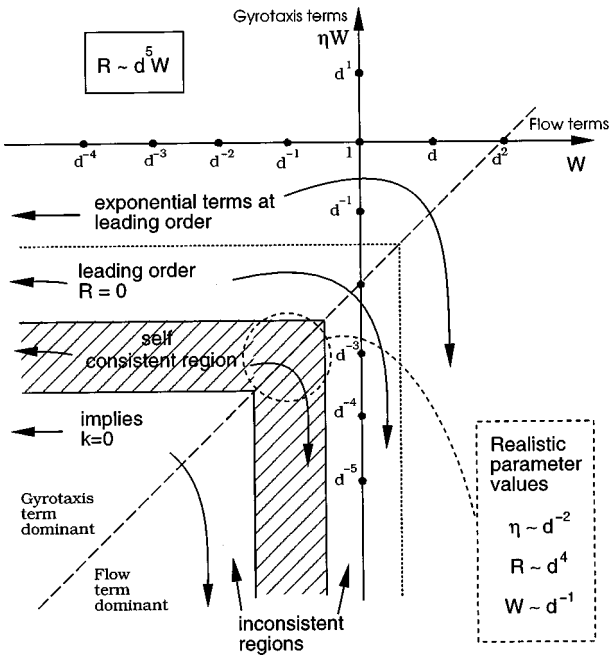

FIG. 2. Regions of parameter space corresponding to leading order balances of the linear equations for bioconvection in a deep layer ($d \gg 1$). The shading indicates the self-consistent region of parameter space where a neutral curve can exist.

which, when expanding Φ in powers of d^{-1} and applying the boundary conditions at $z=-1$, implies that $\Phi=0$. We also have

$$(D^2-k^2)^2 W=0, \tag{51}$$

with $W=DW=0$ on $z=-1$ which implies

$$W=-kA(z+1)\cosh k(z+1) + [A+B(z+1)]\sinh k(z+1), \tag{52}$$

where A and B are constants and can be formally expanded in terms of d^{-1}.

Now consider the inner region. We have

$$(D_I^2-d^{-2}k^2)^2 W=-d^{-5}Rk^2\Phi \tag{53}$$

and

$$(P_V D_I^2-P_V D_I-P_H k^2 d^{-2})\Phi = e^{z_I} d[d^{-2}-\eta P_5 D_I^2-\eta P_6 D_I+\eta P_7 k^2 d^{-2}]W, \tag{54}$$

where $z_I=dz$ and D_I is the operator d/dz_I. The boundary conditions become $(D_I-1)\Phi=W=D_I W=0$ on $z_I=0$. The first equation implies that for a nontrivial solution $R\sim d^5 W$. The second equation is complicated by the exponential term $e^{z_I}\sim 1$ and hence we examine the parameter ranges where the right hand side does not appear at leading order. Assuming $\Phi\sim 1$, we require $W\leqslant O(1)$ and $\eta W\leqslant O(d^{-2})$ for the exponential term not to appear at leading order. We are investigating the equations for the case when $\sigma=0$ (the neutral curve) so we expect there to be only a limited region of parameter space where the equations remain self-consistent. This region is given in Fig. 2. We are restricted to this region due to the balance of terms in Eq. (54) at third order, for which the term $-P_H k^2\Phi_0$ first appears. If there are no terms on the right hand side, then we are led to the solvability condition $P_H k^2=0$ which is unhelpful. If there are terms on the right hand side before third order, then the solvability condition yields $R=0$ or $\eta=0$ at leading orders which is again unhelpful. Thus, restricting attention to the L-shaped region shown in Fig. 2, we immediately see that, as η increases (allowing $R\sim d^5 W$ to vary), R initially remains constant but at some value of η the gyrotactic terms become important and $R(k=0)$ starts decreasing. Considering $W\sim d^{-n}$ where $n=1,2,3,\ldots$, and writing

$$W=\sum_{m=n}^{\infty} W_{-m} d^{-m}, \quad \Phi=\sum_{m=0}^{\infty} \Phi_{-m} d^{-m} \tag{55}$$

and

$$R=d^{5-n}R_{5-n}+d^{5-n-1}R_{5-n-1}+\cdots, \tag{56}$$

then, to first order,

$$D_I^4 W_{-n}+R_{5-n}k^2\Phi_0=0 \quad \text{and} \quad P_V D_I(D_I-1)\Phi_0=0, \tag{57}$$

with appropriate boundary conditions. This has solutions

$$W_{-n}=a_{-n}z_I^3+b_{-n}z_I^2+R_{5-n}k^2(z_I+1-e^{z_I}) \quad \text{and} \quad \Phi_0=e^{z_I}, \tag{58}$$

where the a's and b's are constants. At second order,

$$D_I^4 W_{-n-1}+R_{5-n}k^2\Phi_{-1}=-R_{5-n-1}k^2\Phi_0 \quad \text{and} \quad P_V D_I(D_I-1)\Phi_{-1}=0, \tag{59}$$

and boundary conditions at $z=0$, which has a solution,

$$W_{-n-1}=a_{-n-1}z_I^3+b_{-n-1}z_I^2+R_{5-n-1}k^2(z_I+1-e^{z_I}) \quad \text{and} \quad \Phi_{-1}=0. \tag{60}$$

On matching the inner and outer solutions up to second order in the usual manner (see Kevorkian and Cole[35]) we find that $a_{-n}=a_{-n-1}=b_{-n}=0$,

$$(A_0+B_0)\sinh k - kA_0 \cosh k = 0, \tag{61}$$

$$B_0 \sinh k + B_0 k \cosh k - k^2 A_0 \sinh k = k^2 R_{5-n} \tag{62}$$

and

$$-k^3\frac{\cosh k}{2}A_0 - k^2\frac{\sinh k}{2}A_0 + k^2\frac{\sinh k}{2}B_0 + k\cosh k B_0 = b_{-n-1}. \tag{63}$$

First consider $n=1$ such that $\eta\sim d^{-2}$. The solvability conditions are obtained by integrating the cell conservation equation from $-\infty$ to 0. At third order this gives

$$R_4=\frac{2P_H}{1-(P_5-P_6)\eta_{-2}}, \tag{64}$$

where P_6 is negative. Therefore, R_4 can be negative for sufficiently large $(P_5-P_6)\eta_{-2}$ and the asymptotics break down. This is similar to the analysis of Hill *et al.*[14] in which, for particular values of the gyrotaxis number, the leading order in the Rayleigh number became singular or negative.

Solving for the constants (corrected from Hill *et al.*[14]) we get

$$A_0=\frac{k^2\sinh kR_4}{k^2-\sinh^2 k}, \quad B_0=\frac{(k\cosh k-\sinh k)k^2R_4}{k^2-\sinh^2 k} \tag{65}$$

and

$$b_{-2}=\frac{(k-\cosh k \sinh k)k^3R_4}{k^2-\sinh^2 k}. \tag{66}$$

To find the k dependence, we consider the solvability condition at fourth order and obtain

$$R_3=\frac{4b_{-2}}{k^2}, \tag{67}$$

so that

$$R=\frac{2P_Hd^4}{1-(P_5-P_6)\eta_{-2}}\left[1+4d^{-1}k\frac{(k-\sinh k\cosh k)}{k^2-\sinh^2 k}+O(d^{-2})\right]. \tag{68}$$

This is a monotonically increasing function of k and implies that, for $k\leqslant O(1)$, the most unstable wavenumber is zero. The expression does not say anything about the global most unstable wavenumber for general k.

It is easy to show that we can cover the whole region in parameter space by reducing the importance of certain terms. Going left in parameter space where $\eta\sim d^{-2}$ and $W\sim d^{-1}$ we get that the solvability condition at third order gives

$$R_3=-\frac{2P_H}{(P_5-P_6)\eta_{-1}}, \tag{69}$$

which implies that the asymptotics are not valid for small values of k. We clearly need to balance the advection and gyrotaxis terms, and not let the gyrotaxis terms dominate, to keep the Rayleigh number finite for small k. Going down in the L-shaped region ($\eta\sim d^{-3}$ and $W\sim d^{-1}$) the solvability conditions give

$$R=2P_Hd^4\left[1+d^{-1}\left(\eta_{-3}(P_5-P_6)+\frac{4k(k-\sinh k\cosh k)}{k^2-\sinh^2 k}\right)+O(d^{-2})\right]. \tag{70}$$

This function is a monotonically increasing function of k and gives a most unstable wavenumber of zero [for small k $\leqslant O(1)$].

V. NUMERICAL ANALYSIS

In this section we pursue solutions to the full linear equations with a fourth order finite difference scheme, supplied by Dr. D. R. Moore (see Cash and Moore[36]), that iterates using the Newton-Raphson-Kantorovich algorithm. The program searches for the neutral curves of the equations given initial guesses for the concentration and velocity fields, Φ and W, and the Rayleigh number, R, and it was implemented in a similar manner to that described in Hill *et al.*[14] Up to eighty-one grid points were used to obtain convergent solutions, but this was not always necessary, and stretched meshes were employed to resolve the boundary layer at the upper surface in deep layers. An accuracy of six significant figures was always achieved for convergence. There are a number of parameters that can be varied. P_V and P_H are functions of the parameter λ alone but P_5, P_6 and P_7 are functions of λ and α_0. d is the nondimensional layer depth, $\eta(d)$ is the gyrotactic orientation parameter, k is the wavenumber and $R(d,k,\eta,\lambda,\alpha_0)$ is the Rayleigh number based on the whole suspension depth and is the eigenvalue to be determined. We chose to fix $\lambda=2.2$ (following Pedley and Kessler[15]) thus leaving four parameters to vary. Figures 3–5 show comparisons between the numerical and asymptotic solutions for selected values of d. The values of the parameters have been chosen so that comparisons with Hill *et al.*[14] can be made. Good agreement was always obtained between the asymptotic and numerical solutions for $k\leqslant O(1)$, provided that either $d\ll 1$ (for shallow layers) or $d^{-1}\ll 1$, P_i (for deep layers).

For shallow layers ($d\ll 1$) wavenumbers $>d$ are destabilized with increasing η and wavenumbers $<d$ are very slightly stabilized (Fig. 3). The most unstable wavenumber is nonzero for sufficiently large $d^2\eta$. Figure 6 shows the flow and concentration profiles for a mode one solution, where it can be seen that the perturbations act over the whole suspension layer and are almost symmetrical. For deep layers ($d\gg 1$) the perturbations are greatest towards the upper surface (Fig. 7). For deep layers, large wavenumbers are destabilized and small wavenumbers are stabilized with increasing η. In particular, we find that for $\eta=0$, the most unstable wavenumber is zero but as η increases and exceeds some critical

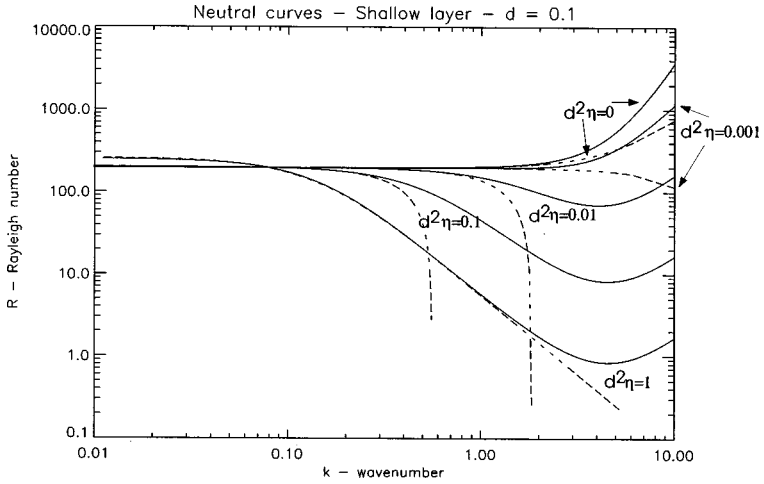

FIG. 3. Curves of neutral linear stability for a shallow layer ($d=0.1$ and $\alpha_0=0.2$) as $d^2\eta$ is varied. Dotted lines are asymptotic results and solid lines are numerical results.

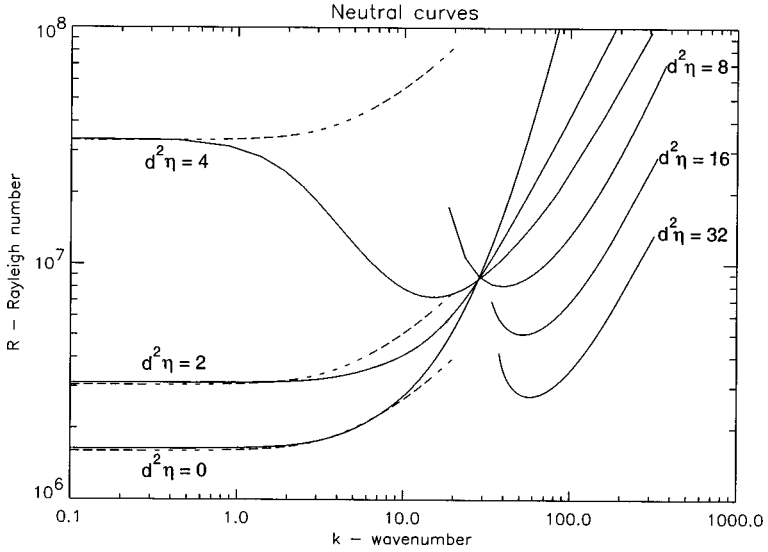

FIG. 4. Curves of neutral linear stability for a deep layer ($d=40$ and $\alpha_0=0.2$) as $d^2\eta$ is varied. Dotted lines are asymptotic results and solid lines are numerical results.

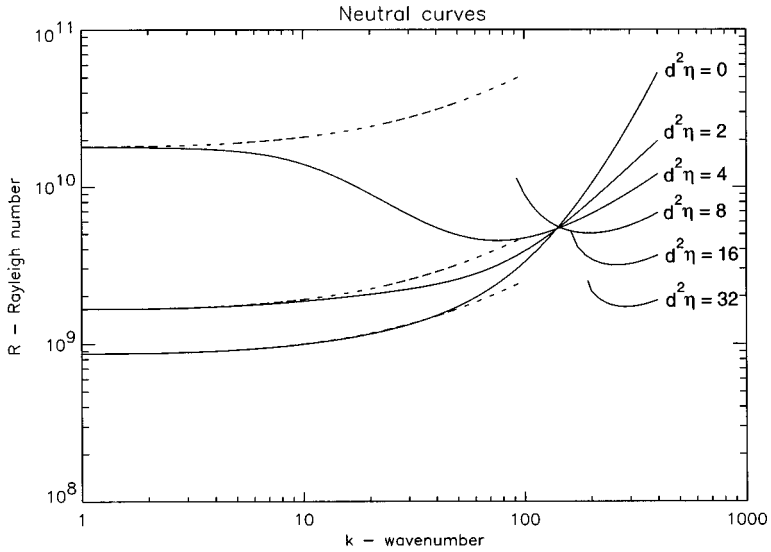

FIG. 5. Curves of neutral linear stability for a deep layer ($d=200$ and $\alpha_0=0.2$) as $d^2\eta$ is varied. Dotted lines are asymptotic results and solid lines are numerical results.

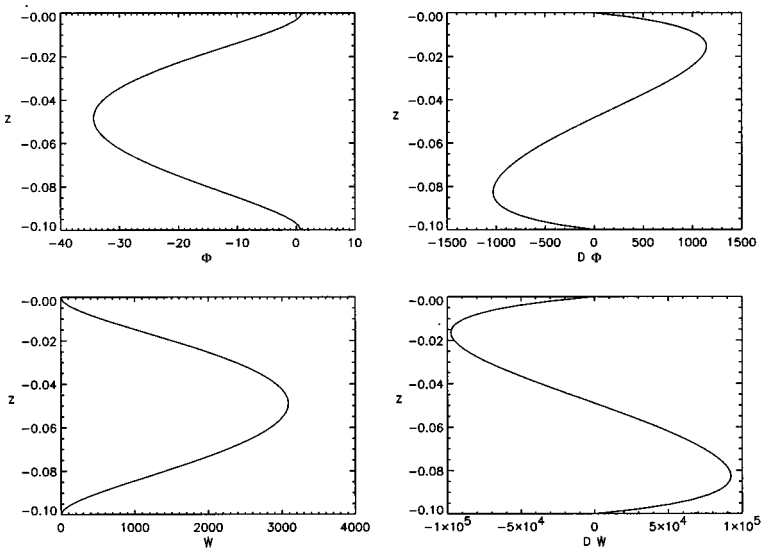

FIG. 6. Profiles of a neutrally stable numerical solution for a shallow layer ($d=0.1$) with $\eta=0.1$, $\alpha_0=0.2$ and $k=10$, for which $R\approx 1155$. This is a mode one solution.

value the most unstable wavenumber jumps to a nonzero value. The asymptotics presented here can not predict the critical value or the nonzero most unstable wavenumber since it is $\geqslant O(1)$. Figure 8 shows a neutral curve where it is clear that minima occur at both a zero and a nonzero wavenumber. As η increases still further $R(k=0)\to\infty$. The value of η for which $R(k)\to\infty$ first as $k\to 0$ can be calculated from the asymptotic analysis [Eq. (68)] to be

$$\eta_c=\frac{d^{-2}}{P_5-P_6}. \tag{71}$$

If $\lambda=2.2$ and $\alpha_0=0.2$ then $d^2\eta_c\approx 4.2$. The asymptotic analysis also suggests that in all cases where $\eta<\eta_c$ the neutral curve increases slightly with k for $k\leqslant O(1)$ before increasing or decreasing when $k>O(1)$. Figure 9 describes the dependence of the neutral curve on α_0. The value of α_0 does not affect the neutral curve significantly for large k but increasing α_0 stabilizes modes with long length scales. This is due to the decrease in P_5 and P_6 when α_0 increases. Elongated cells (i.e., those with large values of α_0) tend to be aligned in one direction in the presence of sufficiently large shear flow (Bees *et al.*[30]). At the onset of a large wavelength instability, for which the streamlines are mainly horizontal, they will swim in almost exactly the opposite direction to the fluid flow (without tumbling, as would occur when $\alpha_0=0$), thus inhibiting the growth of the disturbance.

The Rayleigh number, R, based on the suspension depth, H, is related to the Rayleigh number, $\hat{R}$, based on the sublayer depth, κ^{-1}, by the equation

$$R=d^3\hat{R}. \tag{72}$$

Childress *et al.*[11] found that, in their model for two rigid boundaries (for isotropic diffusion), the critical value of their Rayleigh number, $\hat{R}_c$, behaved like $720/d^4$ for small d and $\hat{R}_c$ decreased to 2 as $d\to\infty$. For free-rigid boundary conditions they found that $\hat{R}_c\sim 320/d^4$ for small d and $\hat{R}_c\sim 4/d$ for large d. Hill *et al.*[14] derive an equation in their asymptotic analysis similar to Eq. (68) which describes the behavior of the neutral curve close to $k=0$. For small k,

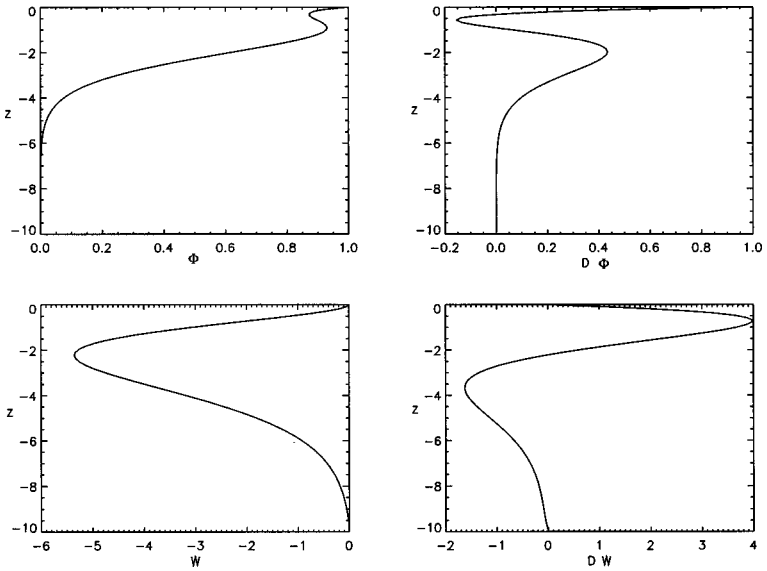

FIG. 7. Profiles of a neutrally stable numerical solution for a deep layer ($d=10$) with $\eta=0.1$, $\alpha_0=0.2$ and $k=10$, for which $R\approx 22024$. This is a mode one solution.

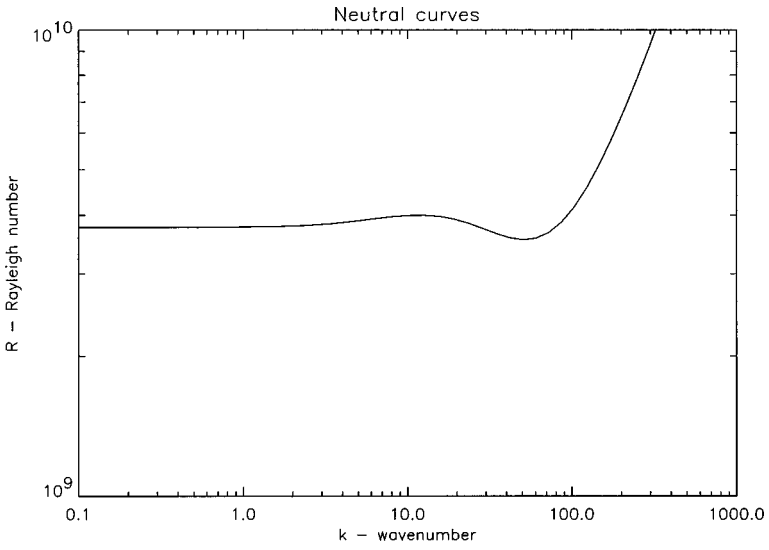

FIG. 8. Numerical curve of neutral linear stability for a deep layer ($d=200$), with $d^2\eta=3.3$, $\alpha_0=0$. Here we see a combination of both zero and nonzero dominant unstable wavenumbers. For every d we find that there is a critical η that determines the bifurcation between there being a zero and a nonzero most unstable wavenumber.

$$R\approx\frac{2P_H d^4}{1-(P_5-P_6)\hat{\eta}}, \tag{73}$$

where the depth independent gyrotaxis number is defined as

$$\hat{\eta}=d^2\eta. \tag{74}$$

Equation (73) is only valid for small enough $\hat{\eta}$, but we measure from Figs. 4 and 5 that if d is large and $\hat{\eta}=33$ then the minimum of the neutral curve is a factor of 2 larger than the value when $\hat{\eta}=0$. Hence, the critical Rayleigh number is given by $R_c\sim 4P_H d^4$. Therefore, we find (as the qualitative results of Hill *et al.*[14] also suggest) that $\hat{R}_c/d$ is initially large and decreases to a constant value as $d\to\infty$. From Figs. 3–5 we find that if $\hat{\eta}=33$ then $\hat{R}_c/d=300$ for $d=0.1$, $\hat{R}_c/d=1.17$ for $d=40$ and $\hat{R}_c/d=1.12$ for $d=200$. The approximate limit of $\hat{R}_c/d$, from above, of $4P_H$ is equal to 1.04.

The theoretically determined nondimensional pattern wavenumber is seen from Figs. 3–5 to decrease with increasing depth. After scaling with $H\approx 2.3\times 10^{-3}d$ cm, we find that the dimensional pattern wavelength increases with depth, but tends to a finite value for large H (keeping $d^2\eta$ constant). This agrees with the measurements of Bees and Hill.[9]

VI. THE EFFECT OF SWIMMING SPEED AS A RANDOM VARIABLE

It is clear from the discussion given in Pedley and Kessler[15] that randomness in the cell swimming direction is important for a number of reasons. Most importantly it alters the mean cell response to the external torques and changes the form of the diffusion tensor. It is necessary to include these factors in the model for the sake of consistency. From the previous section, it is also apparent that the linear behavior of the diffusion tensor, and hence the existence of a non-

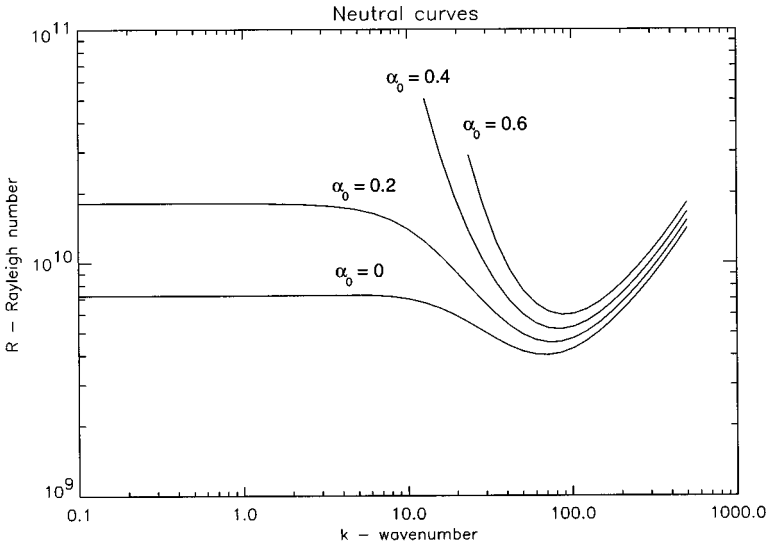

FIG. 9. Numerical curves of neutral linear stability for a deep layer ($d=200$), with $d^2\eta=4$, as α_0 varies. Increasing α_0 stabilizes modes with long horizontal wavelengths.

zero most unstable wavenumber, is dependent on the balance between deterministic processes and randomness in the cell swimming direction. But how else does the cell swim in a random manner? A feature that has been overlooked so far is that the individual cells swim at vastly different speeds. In the real world, with inhomogeneous cultures of *C. nivalis*, there will be large variations in cell swimming speed corresponding to different stages in the cells' life. Hill and Häder[29] investigated both cell swimming speed and orientation. They found that experimental calculations of swimming speed were dependent on the choice of time step size between measurements of position. The cells swim in a smooth fashion and their mean swimming direction is affected by the various taxes. In two experiments Hill and Häder[29] tracked swimming micro-organisms, first in a vertical plane and then in a horizontal plane. Both planes were of small focal depths. Using new techniques of data analysis they were able to calculate mean cell swimming velocities and standard deviations as functions of the time step size and orientation. The data were extrapolated back to a time step size of zero to give the actual swimming velocities. For the vertical plane $\langle V\rangle = 52 \pm 5\ \mu\text{ms}^{-1}$ with a standard deviation of $30 \pm 5\ \mu\text{m s}^{-1}$ and for the horizontal plane $\langle V\rangle = 65 \pm 5\ \mu\text{m s}^{-1}$ with a standard deviation of $30 \pm 5\ \mu\text{m s}^{-1}$.

Theoretically we begin by considering again the calculation for the diffusion tensor $\mathbf{D}$ given in Eq. (13) and assume that it takes a cell τ seconds to settle to a preferred direction (the direction correlation time). Hence,

$$\mathbf{D} = \tau(\langle \mathbf{VV}\rangle - \langle \mathbf{V}\rangle^2), \tag{75}$$

where $\mathbf{V}$ is a random variable (see Bees *et al.*[30]). Assuming that the swimming speed, V, and swimming direction, $\mathbf{p}$, are independent, we can write $\mathbf{V} = V\mathbf{p}$. Given that $\langle V\rangle = V_s$,

$$\mathbf{D} = V_s^2 \tau \left(\frac{\langle V^2\rangle}{V_s^2} \langle \mathbf{pp}\rangle - \langle \mathbf{p}\rangle^2 \right). \tag{76}$$

By varying the ratio

$$\mathcal{N} = \frac{\langle V^2\rangle}{V_s^2}, \tag{77}$$

we can change the nature of the diffusion tensor. The data of Hill and Häder[29] give $\mathcal{N}$ as bounded by 1.15 and 1.45. From Eq. (30), we calculate the modified diffusion tensor to be

$$\frac{1}{V_s^2\tau}\mathbf{D} = \begin{pmatrix} \frac{K_1}{\lambda}\mathcal{N} & 0 & 0 \\ 0 & \frac{K_1}{\lambda}\mathcal{N} & 0 \\ 0 & 0 & \left(1 - \frac{2K_1}{\lambda}\right)\mathcal{N} - K_1^2 \end{pmatrix} + \epsilon \left[\eta(J_2\mathcal{N} - J_1K_1) \begin{pmatrix} 0 & 0 & \omega_2^1 \\ 0 & 0 & -\omega_1^1 \\ \omega_2^1 & -\omega_1^1 & 0 \end{pmatrix} \right.$$
$$\left. -2\alpha_0\eta \begin{pmatrix} [-\frac{3}{4}e_{33}^1K_5 + \frac{1}{4}(e_{11}^1 - e_{22}^1)J_6]\mathcal{N} & \frac{1}{2}e_{12}^1J_6\mathcal{N} & e_{13}^1(J_5\mathcal{N} - K_1J_4) \\ \frac{1}{2}e_{12}^1J_6\mathcal{N} & [-\frac{3}{4}e_{33}^1K_5 - \frac{1}{4}(e_{11}^1 - e_{22}^1)J_6]\mathcal{N} & e_{23}^1(J_5\mathcal{N} - K_1J_4) \\ e_{13}^1(J_5\mathcal{N} - K_1J_4) & e_{23}^1(J_5\mathcal{N} - K_1J_4) & \frac{3}{2}e_{33}^1(K_5\mathcal{N} - 2K_1K_4) \end{pmatrix} \right] + O(\epsilon^2). \tag{78}$$

Substituting the diffusion tensor into the governing equations, we find that only the definitions of the P_i are altered. If $\lambda = 2.2$, these become

$$\begin{aligned} P_H &= 0.26\mathcal{N}, \\ P_V &= 0.48\mathcal{N} - 0.33, \\ P_5 &= 0.38 - 0.21\alpha_0 - \mathcal{N}(0.16 - 0.20\alpha_0), \\ P_6 &= \alpha_0(-0.43 + 0.33\mathcal{N}), \\ P_7 &= 0.38 - 0.22\alpha_0 - \mathcal{N}(0.16 - 0.13\alpha_0). \end{aligned} \tag{79}$$

P_6 is the only term which can change sign for $\mathcal{N} < 2$ and it does so if $\mathcal{N} = 1.3$. This is the average of the bounds on $\mathcal{N}$ determined above from the experiments of Hill and Häder.[29] If $\alpha_0 = 0.4$ and $\mathcal{N} > 3.75$ then two of the parameters will have changed sign and this will have a major effect on the linear analysis. It is, however, unlikely that $\mathcal{N}$ could be so large. Figure 10 describes how the neutral curve varies as a function of $\mathcal{N}$ given η and α_0. The ratio of the leading order horizontal and vertical diffusions,

$$P_H/P_V \approx \frac{0.26\mathcal{N}}{0.48\mathcal{N} - 0.33}, \tag{80}$$

also has some significance. If $\mathcal{N} = 1$ then the ratio is greater than one (as discussed in Pedley *et al.*[15]), but if $\mathcal{N} > 1.5$ then the ratio is less than one (as proposed in Childress *et al.*[11]). Clearly, the true nature of the diffusion tensor and, hence, the value of $\mathcal{N}$ should be established by independent experiments. Thus, the evidence for the sign of P_6 is inconclusive. Perhaps the best that we can do is to assume that P_6 is small, even when d is large, and take $P_6 = 0$ in the analysis. This is not altogether convincing and more accurate experiments

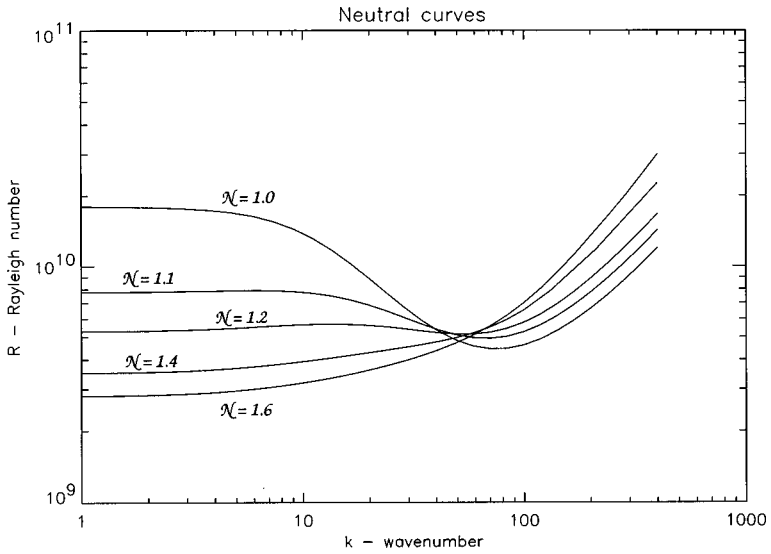

FIG. 10. Neutral curves for a deep layer ($d=200$) where $d^2\eta=4$, $\alpha_0=0.2$ and $\mathcal{N}$ varies.

may need to be performed to elucidate the problem. Alternatively, a better approximation to the diffusion tensor might improve the situation.

As a further example of modeling swimming speed as a random variable, suppose that V is given by a Gamma distribution,

$$P(V=v)=\frac{1}{\Gamma(\xi)}\zeta^{\xi}v^{\xi-1}e^{-\zeta v}, \tag{81}$$

where $v\in[0,\infty)$ and ξ and ζ are parameters. Kessler[37] has been using this distribution to fit data obtained for the swimming speed of bacteria. We find that

$$\mathbf{D}=V_s^2\tau\left(\frac{\xi+1}{\xi}\langle\mathbf{pp}\rangle-\langle\mathbf{p}\rangle^2\right), \tag{82}$$

and, hence $P_6=0$ when $\xi\approx 3.3$.

To obtain results for our best estimates for the parameters, we note that Jones *et al.*[38,39] suggest that allowances may be made for the swimming behavior of *C. nivalis* and the effects of its flagella by increasing α_0 to 0.40 and B to 6.3 s. Also, it has been suggested (Pedley and Kessler[15]) that the value of 1.3 s used above of the direction correlation time, τ, is ''significantly shorter than the observational estimate of 5 s'' and so, here, we take $\tau=5$ s. We choose to take $\mathcal{N}=1.3$ so that $P_6=0$. Neutral curves for the updated parameter ranges are displayed in Fig. 11 where it can be seen that, for the realistic parameter value of $\eta=16d^{-2}$, there is most definitely a nonzero most unstable wavenumber and a reduction in this value dramatically alters the neutral curve such that zero becomes the most unstable wavenumber for $\eta\approx 4d^{-2}$. Given a large enough value of $d^2\eta$, a nonzero most unstable wavenumber will always exist for all d. Figure 11 has the same general characteristics of the previous curves but has a diminished response to an increase in η due to the reduction in (P_5-P_6).

VII. COMPARISON WITH EXPERIMENTS

Pedley and Kessler[15] use the data of Hill and Häder[29] to calculate λ as lying between 1.85 and 2.63. They choose to

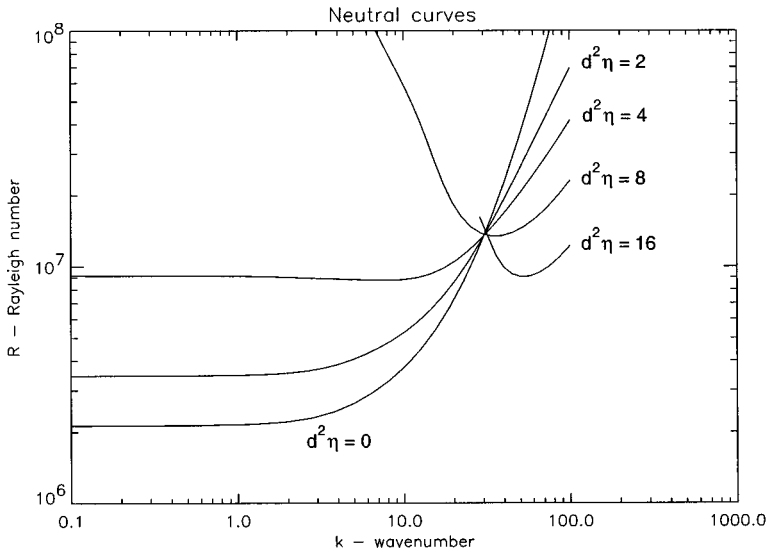

FIG. 11. Neutral curves for $d=40$ using parameter estimates and measurements of $\alpha_0=0.4$ and $\mathcal{N}=1.34$.

TABLE IV. Calculations of parameters from original and more recent measurements and estimates of B and τ.

τ	B	κ	d	R	η
1.3	3.4	435	$435H$	$9170H^5\overline{n}$	$33d^{-2}$
5	6.3	113	$113H$	$161H^5\overline{n}$	$16d^{-2}$

take an average value, as we shall, of 2.2. As we know B from Table II, we can calculate D_r to be 0.067 s^{-1}. The cell eccentricity, α_0, is in the range 0.2–0.31 but Jones[34] has calculated an effective α_0 of 0.40 to allow for the cells' flagella and swimming characteristics. The direction correlation time, τ, can be calculated from observations of the horizontal diffusion to be 1.3 s (Pedley and Kessler[15]), but see Sec. VI where we use a direct observational estimate of 5 s.

Bees and Hill[9] have measured the wavelengths of the first instabilities to arise in a well-mixed suspension of *C. nivalis* as a function of cell concentration and suspension depth. They recorded images of the bioconvection patterns (in low light conditions to avoid the effects of phototaxis) every 10 seconds and applied a Fourier analysis to determine the dominant pattern wavelength as a function of time. They then extracted the wavelength of the first instability to occur. Results were obtained over a wide range of cell concentrations and suspension depths in order to quantify the bioconvection patterns. Although we have no way of drawing a neutral curve from the experiments, because we have no reliable data for the nonexistence of the pattern (especially as d changes with each experiment) the data points from Bees and Hill[9] should lie above the neutral curve for a given measured value of d. Here, we are assuming that the initially observed pattern consists of rolls (as we can reasonably assume from Bees and Hill[9]).

We summarize the theoretical critical values of the Rayleigh numbers and wavenumbers in Table VI, as determined above.

Before direct comparisons are made between the theoretical predictions and the experimental data, it is necessary to investigate some important time-scales. Firstly, we must establish whether the flows caused by the initial mixing have diminished and secondly, we must consider whether the cells have had sufficient time to form the exponential equilibrium

TABLE V. Experimental measurements of wavenumbers (from Bees and Hill[9]) and corresponding calculations of d and R depending on the value of τ. Seven experiments have been chosen with similar depths so that they can be compared with the theoretical predictions.

Experiment name	λ_0 (cm)	$\tilde{\chi}_0$	$\tilde{k}_0$	d	$R(\times 10^6)$	d	$R,(\times 10^6)$
				$\tau=1.3$ s		$\tau=5$ s	
2	0.486	1.23	5.11	172	185	44.7	3.25
4	0.468	1.05	5.98	193	484	50.2	8.50
7	0.417	1.05	5.98	174	82.2	45.2	1.44
17	0.708	1.51	4.16	204	393	53.07	6.90
18	0.354	0.755	8.32	204	393	53.0	6.90
19	0.603	1.29	4.87	204	393	53.0	6.90
23	0.375	0.801	7.84	204	863	53.0	15.2

TABLE VI. Theoretical predictions of critical wavenumbers and critical Rayleigh numbers (to 2 s.f.) for a selection of parameter values. The numbers in brackets indicate the second critical value at the crossover when there are two global minima.

d	$d^2\eta$	α_0	$\mathcal{N}$	k_c	R_c
0.1	0.0	0.2	1.0	0.0	190
0.1	0.001	0.2	1.0	0.0	190
0.1	0.01	0.2	1.0	4.0	70
0.1	0.1	0.2	1.0	4.3	8.3
0.1	1.0	0.2	1.0	4.4	0.81
40	0.0	0.2	1.0	0.0	1.6×10^6
40	2.0	0.2	1.0	0.0	3.1×10^6
40	4.0	0.2	1.0	14	7.1×10^6
40	8.0	0.2	1.0	40	8.0×10^6
40	16	0.2	1.0	51	5.0×10^6
40	32	0.2	1.0	56	2.6×10^6
200	0.0	0.2	1.0	0.0	0.87×10^9
200	2.0	0.2	1.0	0.0	1.6×10^9
200	3.3	0.2	1.0	50 (0.0)	3.3×10^9
200	4.0	0.2	1.0	74	3.3×10^9
200	8.0	0.2	1.0	200	4.0×10^9
200	16	0.2	1.0	240	3.1×10^9
200	32	0.2	1.0	270	1.7×10^9
200	4.0	0.0	1.0	65	4.0×10^9
200	4.0	0.2	1.0	75	4.4×10^9
200	4.0	0.4	1.0	82	5.1×10^9
200	4.0	0.6	1.0	88	6.0×10^9
200	4.0	0.2	1.0	75	4.4×10^9
200	4.0	0.2	1.1	66	5.0×10^9
200	4.0	0.2	1.2	52 (0.0)	5.1×10^9
200	4.0	0.2	1.4	0	3.4×10^9
200	4.0	0.2	1.6	0	2.8×10^9
40	0.0	0.4	1.34	0.0	2.1×10^6
40	2.0	0.4	1.34	0.0	3.3×10^6
40	4.0	0.4	1.34	7.7	8.7×10^6
40	8.0	0.4	1.34	33	13×10^6
40	16	0.4	1.34	51	9.0×10^6

solution as assumed in this linear analysis. A similar argument was presented by Hill *et al.*[14] We assume that the petri dish and suspension are in solid body rotation with angular velocity $\mathbf{\Omega}$ until the container is instantaneously brought to rest. The time for spin-down of the suspension is $O(E^{1/2}|\mathbf{\Omega}|^{-1})$ where E is the Ekman number so that if $|\mathbf{\Omega}| \sim 1$ s^{-1} then the decay time is approximately 10 s. If we take the cell swimming speed to be 63 μm s^{-1} upwards (Table II) then the cells would require 100 s to swim a typical depth of 6 mm from bottom to top. The cells typically form patterns 30 s after the initial mixing. Hence, we can assume that the majority of the fluid motion due to mixing has decayed away before the onset of instability but that the cells do not always have sufficient time to swim and form the exponential equilibrium profile assumed in the linear analysis of this paper. In some situations in which the suspension is deep it may be more appropriate to use the linear analysis of Pedley and Kessler[15] (see Bees and Hill[40]).

Seven experiments share a similar depth of approximately 0.4 cm, for which $d\approx200$ if $\tau=1.3$ s and $d\approx40$ if $\tau=5$ s. These results can be compared directly with existing results from the linear analysis. In computing Table IV, the following expressions for d, R and κ were used in conjunction with Table II,

$$d=\kappa H, \tag{83}$$

$$R=\frac{\upsilon g\Delta\rho\kappa^2}{\nu\rho V_s^2\tau}\left(\frac{H^5\overline{n}}{1-e^{-\kappa H}}\right) \tag{84}$$

and

$$\kappa=\frac{K_1}{K_2V_s\tau}. \tag{85}$$

As

$$\eta=\frac{BV_s^2\tau}{H^2}=\frac{BV_s^2\tau\kappa^2}{d^2}, \tag{86}$$

and if $\tau=1.3$ s and $B=3.4$ s (the original estimates), then $\eta\approx 33d^{-2}$. For the new estimates of $\tau=5$ s and $B=6.3$ s (see Jones[37]), $\eta=16d^{-2}$.

Comparing the data from the $\tau=1.3$ s and $\tilde{k}_0$ columns of Table V with Fig. 5 for $\eta=32d^{-2}$, we find that the measured Rayleigh numbers are all less than the minimum value, 2×10^9, of the neutral curve. Also, the wavenumbers are 20 to 40 times smaller than the predicted values. Comparing the data from the $\tau=5$ s and $\tilde{k}_0$ columns of Table V with Fig. 11 reveals that the measured Rayleigh numbers are now of comparable order to the neutral curve but the measured wavenumbers are 5 to 10 times smaller than those predicted. Reducing η to $4d^{-2}$ would have the desirable effect of making the predicted most unstable wavenumber be similar to the measured value. In general, increasing τ and decreasing B improves the agreement between experiments and theoretical predictions. It is also possible to adjust other parameters in the Rayleigh number such that the neutral curve coincides more precisely with the measured data points but the choice of values would be somewhat arbitrary and it should be the priority of experimental work to establish more precise independent measurements of these parameters. The stochastic and deterministic models of gyrotactic bioconvection differ in their quantitative predictions of initial pattern wavelengths. Typically Hill *et al.*[14] predict a wavelength of 2 to 3 cm in a suspension of depth 1 cm and we predict a wavelength of approximately 1 mm. Experimental measurements give a typical wavelength of between 4 and 7 mm, halfway between the two predictions. Better agreement can be obtained by using τ and B as tuning parameters.

VIII. CONCLUSION

We have examined the linear stability of bioconvection patterns for a finitely deep suspension of swimming microorganisms using the ''new'' continuum model of Pedley and Kessler.[15] The importance of treating the swimming speed as an independent random variable has been brought out. Many parameters have to be estimated and, from these estimates, good agreement with the experiments of Bees and Hill[9] is obtained that is a general improvement on the earlier analysis of Hill *et al.*[14] Perfect agreement can be obtained by fitting the theory to the experimental data with choices of parameters within realistic bounds. However, future experiments should concentrate on obtaining independent measurements of the parameters in order to validate the theory. Nonlinear aspects of bioconvection have been studied using Pedley and Kessler's[15] continuum model and the general-flow solutions of the Fokker-Planck equation[30] in a recent paper by Bees and Hill.[40]

ACKNOWLEDGMENT

M.A.B. would like to acknowledge the financial support of the EPSRC through an Earmarked Award in Mathematical Biology during this work.

APPENDIX A: EXPRESSIONS USED IN LINEAR ANALYSIS

Consider the equilibrium state of no flow where $\mathbf{u}=\omega=\mathbf{e}=\mathbf{0}$ and $f=f^0$. Writing $\mathbf{p}=(\sin\theta\cos\phi,\ \sin\theta\sin\phi,\ \cos\theta)^T$ and $\mathbf{k}=(0,\ 0,\ 1)^T$, gives

$$\frac{1}{\sin\theta}\frac{\partial}{\partial\theta}\left(\sin\theta\frac{\partial f^0}{\partial\theta}\right)+\frac{1}{\sin^2\theta}\frac{\partial^2 f^0}{\partial\phi^2}$$

$$=-\lambda\left(\sin\theta\frac{\partial f^0}{\partial\theta}+2f^0\cos\theta\right). \tag{A1}$$

Assuming axial symmetry and applying the normalization condition over the surface S of the sphere, $\int_S f^0=1$, gives

$$f^0=\mu_\lambda e^{\lambda\cos\theta}, \tag{A2}$$

where

$$\mu_\lambda=\frac{\lambda}{4\pi\sinh\lambda}. \tag{A3}$$

This is a special case of the Fisher distribution on a sphere (see Mardia[41]). Substituting into (11) and (13) gives

$$\langle\mathbf{p}\rangle^0=(0,\ 0,\ K_1)^T, \tag{A4}$$

where

$$K_1=\coth\lambda-\lambda^{-1}, \tag{A5}$$

and

$$\mathbf{D}^0=V_s^2\tau\begin{bmatrix}\frac{K_1}{\lambda} & 0 & 0\\ 0 & \frac{K_1}{\lambda} & 0\\ 0 & 0 & K_2\end{bmatrix}, \tag{A6}$$

where

$$K_2=1-\coth^2\lambda+\frac{1}{\lambda^2}. \tag{A7}$$

Perturbing the equilibrium solution, such that

$$\mathbf{u}=\epsilon\mathbf{u}^1,\quad \boldsymbol{\omega}=\epsilon\boldsymbol{\omega}^1,\quad \mathbf{e}=\epsilon\mathbf{e}^1\quad\text{and}\quad f=f^0+\epsilon f^1, \tag{A8}$$

where $0<\epsilon\ll 1$, in spherical polar coordinates $(\theta,\ \phi)$ at $O(\epsilon)$, Eq. (18) gives

$$\frac{\lambda^{-1}}{\sin\theta}\frac{\partial}{\partial\theta}\left(\sin\theta\frac{\partial f^1}{\partial\theta}\right)+\frac{\lambda^{-1}}{\sin^2\theta}\frac{\partial^2 f^1}{\partial\phi^2}-\mathbf{k}\cdot\hat{\boldsymbol{\theta}}\frac{\partial f^1}{\partial\theta}+2\cos\theta f^1$$
$$=\eta\left(\boldsymbol{\omega}^1\cdot\mathbf{p}\wedge\hat{\boldsymbol{\theta}}\frac{\partial f^0}{\partial\theta}+2\alpha_0\mathbf{p}\cdot\mathbf{e}^1\cdot\hat{\boldsymbol{\theta}}\frac{\partial f^0}{\partial\theta}-6\alpha_0\mathbf{p}\cdot\mathbf{e}^1\cdot\mathbf{p}f^0\right), \tag{A9}$$

where

$$\frac{\partial f^0}{\partial\theta}=-\mu_\lambda\lambda\sin\theta e^{\lambda\cos\theta},$$

$$\hat{\boldsymbol{\theta}}=(\cos\theta\sin\phi,\cos\theta\cos\phi,-\sin\theta)^T,$$

$$\mathbf{p}\wedge\hat{\boldsymbol{\theta}}=(-\sin\theta,\cos\theta,0)^T,$$

$$\mathbf{p}\cdot\mathbf{e}^1\cdot\hat{\boldsymbol{\theta}}=-\tfrac{3}{4}e^1_{33}\sin 2\theta+[\tfrac{1}{4}(e^1_{11}-e^1_{22})\cos 2\phi+\tfrac{1}{2}e^1_{12}\sin 2\phi]\sin 2\theta+[e^1_{13}\cos\phi+e^1_{23}\sin 2\phi]\cos 2\theta$$

and

$$\mathbf{p}\cdot\mathbf{e}^1\cdot\mathbf{p}=\tfrac{1}{2}e^1_{33}(3\cos^2\theta-1)+[\tfrac{1}{2}(e^1_{11}-e^1_{22})\cos 2\phi+e^1_{12}\sin 2\phi]\sin^2\theta+[e^1_{13}\cos\phi+e^1_{23}\sin 2\phi]\sin 2\theta. \tag{A10}$$

This equation is solved using associated Legendre polynomials as in Pedley and Kessler[15] and results in Eqs. (29) and (30) with the following definitions for the constants therein (note, in particular, the amendment to K_4):

$$\mu_\lambda=\frac{\lambda}{4\pi\sinh\lambda},$$
$$K_1=\coth\lambda-\frac{1}{\lambda},$$
$$K_2=1-\coth^2\lambda+\frac{1}{\lambda^2},$$
$$K_3=1-\frac{3K_1}{\lambda},$$
$$K_4=1-\coth^2\lambda-\frac{2K_1}{\lambda}+\frac{\coth\lambda}{\lambda}=K_2-\frac{K_1}{\lambda},$$
$$K_5=-\frac{2}{\lambda}\left[2+\frac{5}{\lambda^2}-\frac{4\coth\lambda}{\lambda}-\coth^2\lambda\right]=-\frac{2}{\lambda}\left[1+K_2-\frac{4K_1}{\lambda}\right], \tag{A11}$$
$$J_1=\frac{4}{3}\pi\lambda\mu_\lambda\sum_{l=0}^{\infty}\lambda^{2l+1}a_{2l+1,1},$$
$$J_2=\frac{4}{5}\pi\lambda\mu_\lambda\sum_{l=1}^{\infty}\lambda^{2l}a_{2l,2},$$
$$J_4=\frac{4}{3}\pi\lambda\mu_\lambda\sum_{l=0}^{\infty}\lambda^{2l+1}\tilde{a}_{2l+1,1}, \tag{A12}$$
$$J_5=\frac{4}{5}\pi\lambda\mu_\lambda\sum_{l=0}^{\infty}\lambda^{2l}\tilde{a}_{2l,2},$$
$$J_6=\frac{16}{5}\pi\lambda\mu_\lambda\sum_{l=0}^{\infty}\lambda^{2l}\bar{a}_{2l,2},$$

where $a,\tilde{a}$ and $\bar{a}$ are defined by

$$a_{nm}=-\frac{m+2}{(m+1)(2m+3)}a_{n-1,m+1}+\frac{m-1}{(2m-1)m}a_{n-1,m-1}+\frac{b_{nm}}{m(m+1)}, \tag{A13}$$

where

$$b_{n+1,m}=\begin{cases}0, & \forall(n+m)\quad\text{even},\\ \dfrac{(2m+1)\Gamma((n+1)/2)\Gamma((n+2)/2)}{4\Gamma(n+1)\Gamma((n-m+3)/2)\Gamma((n+m+4/)2)}, & \forall(n+m)\quad\text{odd};\end{cases} \tag{A14}$$

$$\tilde{a}_{nm}=-\frac{m+2}{(m+1)(2m+3)}\tilde{a}_{n-1,m+1}+\frac{m-1}{(2m-1)m}\tilde{a}_{n-1,m-1}+\frac{\tilde{b}_{nm}}{m(m+1)}, \tag{A15}$$

where

$$\tilde{b}_{n+1,m}=\begin{cases}0, & \forall(n+m)\quad\text{even},\\ -\dfrac{(2m+1)\Gamma((n+1)/2)\Gamma((n+2)/2)(n^2+5n+4+m+m^2)}{16\Gamma(n+1)\Gamma((n-m+5)/2)\Gamma((n+m+6)/2)}, & \forall(n+m)\quad\text{odd};\end{cases} \tag{A16}$$

$$\bar{a}_{nm}=-\frac{m+3}{(m+1)(2m+3)}\bar{a}_{n-1,m+1}+\frac{m-2}{(2m-1)m}\bar{a}_{n-1,m-1}+\frac{\bar{b}_{nm}}{m(m+1)}, \tag{A17}$$

where

$$\overline{b}_{n+1,m}=\begin{cases}0, & \\ -\dfrac{(2m+1)\Gamma((n+2)/2)\Gamma((n+3)/2)(n+4)}{8\Gamma(n+2)\Gamma((n-m+5)/2)\Gamma((n+m+6)/2)}, & \end{cases}$$

$$\begin{aligned}&\forall(n+m) \quad \text{even},\\ &\forall(n+m) \quad \text{odd}.\end{aligned} \tag{A18}$$

To $O(\epsilon)$, the governing equations become

$$\nabla\cdot\mathbf{u}^1=0, \tag{A19}$$

$$S_c^{-1}\frac{\partial\mathbf{u}^1}{\partial t}=-\nabla p_e^1-\gamma n^1\mathbf{k}+\nabla^2\mathbf{u} \tag{A20}$$

and

$$\frac{\partial n^1}{\partial t}=-\nabla\cdot\left[e^{dz}\mathbf{u}^1+d\frac{K_2}{K_1}e^{dz}\langle\mathbf{p}\rangle^1+d\frac{K_2}{K_1}n^1\langle\mathbf{p}\rangle^0-\mathbf{D}^0\cdot\nabla n^1-de^{dz}\mathbf{D}^1\cdot\mathbf{k}\right]. \tag{A21}$$

These five p.d.e.'s in five unknowns are reduced to two p.d.e.'s in two unknowns as follows. Expanding Eq. (A21) we obtain

$$\begin{aligned}\frac{\partial n^1}{\partial t}=&-de^{dz}u_3^1-d\frac{K_2}{K_1}e^{dz}\partial_i\langle\mathbf{p}\rangle_i^1-d^2\frac{K_2}{K_1}e^{dz}\langle\mathbf{p}\rangle_3^1\\&-d\frac{K_2}{K_1}\langle\mathbf{p}\rangle_i^0\partial_i n^1+D_{ij}^0\partial_i\partial_j n^1+D_{33}^1d^2e^{dz}\\&+de^{dz}\partial_i D_{i3}^1,\end{aligned} \tag{A22}$$

where $\partial_i\equiv\partial/\partial x_i$ and repeated indices are summed over 1, 2 and 3. Since $\partial_3(\partial_i u_i^1)=0$, we get

$$\partial_1\omega_2^1-\partial_2\omega_1^1=-\nabla^2u_3^1 \quad \text{and}$$

$$\partial_1 e_{13}^1+\partial_2 e_{23}^1=\tfrac{1}{2}\nabla^2u_3^1-\partial_3\partial_3u_3^1. \tag{A23}$$

Hence, Eq. (29) gives

$$\partial_i\langle\mathbf{p}\rangle_i^1=-\eta(J_1+\alpha_0J_4)\nabla^2u_3^1+\eta\alpha_0(2J_4-3K_4)\partial_3\partial_3u_3^1 \tag{A24}$$

and from Eq. (30) we obtain

$$\begin{aligned}\partial_i D_{i3}^1=&-\eta[J_2-J_1K_1+\alpha_0(J_5-K_1J_4)]\nabla^2u_3^1\\&+\eta\alpha_0[2(J_5-K_1J_4)-3(K_5-2K_1K_4)]\partial_3\partial_3u_3^1.\end{aligned} \tag{A25}$$

Substituting Eqs. (A25) and (A24) into Eq. (A22) yields Eq. (32). Taking the divergence of Eq. (A20), and the Laplacian of the third component of Eq. (A20) we get

$$0=-\nabla^2p_e^1-\gamma\partial_3n^1 \quad \text{and}$$

$$S_c^{-1}\frac{\partial}{\partial t}(\nabla^2u_3^1)=-\partial_3\nabla^2p_e^1+\nabla^2\nabla^2u_3^1-\gamma\nabla^2n^1. \tag{A26}$$

Substituting the former into the latter gives Eq. (31).

APPENDIX B: A SUMMARY OF THE ASYMPTOTIC RESULTS

1. Shallow layer, $d\ll 1$

• $\eta\leqslant O(1)$ Mode one solutions belong to Case Ib where $R\sim 1$ and

$$R^{(1)}=720P_H\left\{1+\frac{1}{2}d+d^2\left(\frac{13}{105}+\tilde{k}^2\left[\frac{1}{21}-\frac{5P_H}{462P_V}\right]\right)\right\}+O(d^3). \tag{B1}$$

Modes of order greater than two belong to Case II and imply that $R\sim d^{-2}$. R for a mode two solution, with similar expressions for higher modes, is given by

$$R^{(n)}=\frac{w_n^6P_V}{\tilde{k}^2}d^{-2}+O(d^{-1}) \tag{B2}$$

where $n=2,3,\ldots$, $w_n=n\pi$ if n is even and $w_n\approx n\pi$ if n is odd.

• $\eta\sim 1$ Modes of order one again come from Case Ib and R is given by

$$R^{(1)}=720P_H\left\{1+\frac{1}{2}d+d^2\left(\frac{13}{105}+\eta(P_5-P_6)+\tilde{k}^2\left[\frac{1}{21}-\frac{5P_H}{462P_V}-\eta\left(P_7+\frac{3P_5P_H}{7P_V}\right)\right]\right)\right\}+O(d^3). \tag{B3}$$

Modes of higher order belong to Case III and it can be seen that

$$R^{(n)}\sim d^{-2}, \tag{B4}$$

where $n=2,3,\ldots$.

• $\eta\sim d^{-1}$ Mode one is from Case Ib,

$$R^{(1)}=720P_H\left\{1+d\left[\frac{1}{2}+\eta_{-1}(P_5-P_6)-\tilde{k}^2\eta_{-1}\left(P_7+\frac{3P_5P_H}{7P_V}\right)\right]\right\}+O(d^2). \tag{B5}$$

Modes of higher orders are from Case IV (where $m=1$),

$$R^{(n)}=\frac{w_n^4P_V}{\tilde{k}^2\eta_{-1}P_5}d^{-1}+O(1), \tag{B6}$$

where $n=2,3,\ldots$, $w_2=5\pi/2$ and $5\pi/2\leqslant w_3\leqslant 9\pi/2$.

• $\eta\sim d^{-2}$ All modes are determined in Case IV and give

$$R^{(n)}=\frac{w_n^4P_V}{\tilde{k}^2\eta_{-2}P_5}+O(d), \tag{B7}$$

where $n=1,2,3,\ldots$. Even modes have a constant w_n with $\tilde{k}$, but odd modes have $w_n=w_n[F(\tilde{k}^2)]$, where $(2n-1)\pi/2\leqslant w_n\leqslant(2n+3)\pi/2$. For $\eta_{-2}<1/P_5$ where $w\to 0$ and $\tilde{k}\in\mathbb{R}$ then

$$R^{(1)}\to\frac{720P_H}{1-(P_5-P_6)\eta_{-2}} \tag{B8}$$

as $\tilde{k}\to 0$.

• $\eta\geqslant O(d^{-m})$ where $m\geqslant 3$. All modes are covered by Case IV,

$$R^{(n)}=\frac{w_n^4P_V}{\tilde{k}^2\eta_{-m}P_5}d^{m-2}+O(d^{m-1}), \tag{B9}$$

where the w_n are given as before.

2. Deep layer, $d\gg 1$

• $\eta\leqslant O(d^{-4})$,

$$R^{(1)}=2P_Hd^4\left[1+d^{-1}\left(\frac{4k}{k^2-\sinh^2 k}(k-\sinh k\cosh k)\right)+O(d^{-2})\right]. \tag{B10}$$

• $\eta\sim d^{-3}$ [Eq. (70)],

$$R^{(1)}=2P_Hd^4\left[1+d^{-1}\left(\frac{4k}{k^2-\sinh^2 k}(k-\sinh k\cosh k)+\eta_{-3}(P_5-P_6)\right)+O(d^{-2})\right]. \tag{B11}$$

• $\eta\sim d^{-2}$ [Eq. (68)],

$$R^{(1)}=\frac{2P_Hd^4}{1-(P_5-P_6)\eta_{-2}}\left[1+d^{-1}\frac{4k(k-\sinh k\cosh k)}{k^2-\sinh^2 k}+O(d^{-2})\right]. \tag{B12}$$

• $\eta\geqslant O(d^{-1})$ [Eq. (69)],

$$R^{(1)}=-\frac{2P_Hd^3}{P_5-P_6\eta_{-1}}+O(d^2), \tag{B13}$$

and asymptotics break down for small k.

[1] J. R. Platt, ''Bioconvection patterns in cultures of free-swimming organisms,'' Science **133**, 1766 (1961).
[2] H. Wager, ''The effect of gravity upon the movements and aggregation of *Euglena viridis, Ehrb.*, and other micro-organisms,'' Philos. Trans. R. Soc. London, Ser. B **201**, 333 (1911).
[3] J. B. Loeffer and R. B. Mefferd, ''Concerning pattern formation by free-swimming microorganisms,'' Am. Nat. **86**, 325 (1952).
[4] W. Nultsch and E. Hoff, ''Investigation on pattern formation in *Euglenae*,'' Arch. Protistenk **115**, 336 (1973).
[5] M. S. Plesset and H. Winet, ''Bioconvection patterns in swimming microorganism cultures as an example of Rayleigh-Taylor instability,'' Nature (London) **248**, 441 (1974).
[6] J. O. Kessler, ''Co-operative and concentrative phenomena of swimming micro-organisms,'' Contemp. Phys. **26**, 147 (1985b).
[7] J. O. Kessler, ''Gyrotactic buoyant convection and spontaneous pattern formation in algal cell cultures,'' in *Non-Equilibrium Cooperative Phenomena in Physics and Related Fields*, edited by M. G. Velarde (Plenum, New York, 1984), pp. 241–248.
[8] M. A. Bees, ''Non-Linear pattern generation in suspensions of swimming micro-organisms,'' Ph.D. thesis, University of Leeds, 1996.
[9] M. A. Bees and N. A. Hill, ''Wavelengths of bioconvection patterns,'' J. Exp. Biol. **200**, 1515 (1997).
[10] M. Levandowsky, W. S. Childress, E. A. Spiegel, and S. H. Hutner, ''A mathematical model of pattern formation by swimming microorganisms,'' J. Protozool. **22**, 296 (1975).
[11] S. Childress, M. Levandowsky, and E. A. Spiegel, ''Pattern formation in a suspension of swimming micro-organisms: Equations and stability theory,'' J. Fluid Mech. **69**, 595 (1975).
[12] J. O. Kessler, ''Hydrodynamic focussing of motile algal cells,'' Nature (London) **313**, 218 (1985a).
[13] T. J. Pedley, N. A. Hill, and J. O. Kessler, ''The growth of bioconvection patterns in a uniform suspension of gyrotactic micro-organisms,'' J. Fluid Mech. **195**, 223 (1988).
[14] N. A. Hill, T. J. Pedley, and J. O. Kessler, ''Growth of bioconvection patterns in a suspension of gyrotactic micro-organisms in a layer of finite depth,'' J. Fluid Mech. **208**, 509 (1989).
[15] T. J. Pedley and J. O. Kessler, ''A new continuum model for suspension of gyrotactic micro-organisms'' J. Fluid Mech. **212**, 155 (1990).
[16] H. Brenner and M. H. Weissmann, ''Rheology of a dilute suspension of dipolar spherical particles in an external field. II. Effects of rotary Brownian motion,'' J. Colloid Interface Sci. **41**, 499 (1972).
[17] H. Brenner, ''Suspension rheology,'' Prog. Heat Mass Transfer **5**, 89 (1972).
[18] H. Brenner, ''Rheology of a dilute suspension of axisymmetric Brownian particles,'' Int. J. Multiphase Flow **1**, 195 (1974).
[19] E. J. Hinch and L. G. Leal, ''The effect of Brownian motion on the rheological properties of a suspension of non-spherical particles,'' J. Fluid Mech. **52**, 683 (1972a).
[20] E. J. Hinch and L. G. Leal, ''Note on the rheology of a dilute suspension of dipolar spheres with weak Brownian couples,'' J. Fluid Mech. **56**, 803 (1972b).
[21] L. G. Leal and E. J. Hinch, ''The effect of weak Brownian rotations on particles in shear flow,'' J. Fluid Mech. **46**, 685 (1971).
[22] L. G. Leal and E. J. Hinch, ''The rheology of a suspension of nearly spherical particles subject to Brownian rotations,'' J. Fluid Mech. **55**, 745 (1972).
[23] S. Chandrasekar, *Hydrodynamic and Hydromagnetic Stability* (Oxford University Press, Clarendon, 1961).
[24] A. J. Hillesdon, T. J. Pedley, and J. O. Kessler, ''The development of concentration gradients in a suspension of chemotactic bacteria,'' Bull. Math. Biol. **57**, 299 (1995).
[25] A. J. Hillesdon, ''Pattern formation in a suspension of swimming bacteria,'' Ph.D. thesis, University of Leeds, 1994.
[26] G. Veronis, ''Penetrative convection,'' Astrophys. J. **137**, 641 (1963).
[27] R. V. Vincent and N. A. Hill, ''Bioconvection in a suspension of phototactic algae,'' J. Fluid Mech. **327**, 343 (1996).
[28] J.-J. Shu, N. A. Hill, and S. Ghorai, ''Diffusion of a dilute suspension of dipolar swimming particles,'' submitted to J. Fluid Mech.
[29] N. A. Hill and D. P. Häder, ''A biased random walk model for the trajectories of swimming micro-organisms,'' J. Theor. Biol. **186**, 503 (1997).
[30] M. A. Bees, N. A. Hill, and T. J. Pedley, ''Analytical approximations for the orientation of small dipolar particles in steady shear flows,'' J. Math. Biol. **36**, 269 (1998).
[31] H. Risken, *The Fokker-Planck Equation*, 2nd ed. (Springer-Verlag, Berlin, 1989).
[32] M. Schienbein and H. Gruler, ''Langevin equation, Fokker-Planck equation and cell migration,'' Bull. Math. Biol. **55**, 585 (1993).
[33] T. J. Pedley and J. O. Kessler, ''Hydrodynamic phenomena in suspensions of swimming micro-organisms,'' Annu. Rev. Fluid Mech. **24**, 313 (1992).
[34] G. B. Jeffrey, ''The motion of ellipsoidal particles immersed in a viscous fluid,'' Proc. R. Soc. London, Ser. A **102**, 161 (1922).
[35] J. Kevorkian and J. D. Cole, *Perturbation Methods in Applied Mathematics* (Springer-Verlag, Berlin, 1981).
[36] J. R. Cash and D. R. Moore, ''A high order method for the numerical solution of two-point boundary value problems,'' BIT **20**, 44 (1980).

[37]J. O. Kessler (private communication, 1995).
[38]M. S. Jones, ''Hydrodynamics of bi-flagellate locomotion,'' Ph.D. thesis, University of Leeds, 1995.
[39]M. S. Jones, L. le Baron, and T. J. Pedley, ''Biflagellate gyrotaxis in a shear flow,'' J. Fluid Mech. **281**, 137 (1994).
[40]M. A. Bees and N. A. Hill, ''Non-linear bioconvection in a deep suspension of gyrotactic micro-organisms,'' to appear in J. Math. Biol.
[41]K. Mardia, *Statistics of Directional Data* (Academic, New York, 1972).